9-15-2020

Design of a Methanol Reformer for on-board Production of Hydrogen as Fuel for a 3kW High-temperature Proton Exchange Membrane Fuel Cell Power System

Vladimir Gurau
Georgia Southern University, vgurau@georgiasouthern.edu

Adedayo Ogunleke
Georgia Southern University, ao5589@georgiasouthern.edu

F. Strickland

Available online at www.sciencedirect.com

ScienceDirect

journal homepage: www.elsevier.com/locate/he

Design of a methanol reformer for on-board production of hydrogen as fuel for a 3 kW High-Temperature Proton Exchange Membrane Fuel Cell power system

V. Gurau [a,*], A. Ogunleke [b], F. Strickland [a]

[a] Georgia Southern University, Department of Manufacturing Engineering, Statesboro, GA, 30458, USA
[b] Georgia Southern University, Mechanical Engineering Department, Statesboro, GA, 30458, USA

HIGHLIGHTS

- CFD is an essential tool for determining process parameters of methanol reformers.
- Operating conditions of MEAs are critical constraints in methanol reformer design.
- Reformer design must result in high conversion efficiency and small reformer volume.

GRAPHICAL ABSTRACT

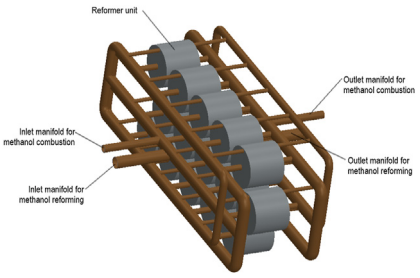

ARTICLE INFO

Article history:
Received 31 January 2020
Received in revised form
28 May 2020
Accepted 21 August 2020
Available online 15 September 2020

Keywords:
Methanol reformer
High-temperature proton exchange membrane fuel cell
Methanol steam reforming
Fuel cell system optimization
Computational fluid dynamics

ABSTRACT

The method of Computational Fluid Dynamics is used to predict the process parameters and select the optimum operating regime of a methanol reformer for on-board production of hydrogen as fuel for a 3 kW High-Temperature Proton Exchange Membrane Fuel Cell power system. The analysis uses a three reactions kinetics model for methanol steam reforming, water gas shift and methanol decomposition reactions on $Cu/ZnO/Al_2O_3$ catalyst. Numerical simulations are performed at single channel level for a range of reformer operating temperatures and values of the molar flow rate of methanol per weight of catalyst at the reformer inlet. Two operating regimes of the fuel processor are selected which offer high methanol conversion rate and high hydrogen production while simultaneously result in a small reformer size and a reformate gas composition that can be tolerated by phosphoric acid-doped high temperature membrane electrode assemblies for proton exchange membrane fuel cells. Based on the results of the numerical simulations, the reactor is sized, and its design is optimized.

* *Corresponding author.*
E-mail address: vgurau@georgiasouthern.edu (V. Gurau).

https://doi.org/10.1016/j.ijhydene.2020.08.179

Nomenclature

A	Active area of the fuel cell MEA (cm^2)
a_{ref}	Specific area density of the reformer catalyst ($3.5 \times 10^8 m^2/m^3$)
c_p	Specific heat capacity at constant pressure ($J/kg\ K$)
$C_1 - C_7$	Adsorption coefficients of surface spices (bar^{-X})
CS_1^T, CS_{1A}^T	Total surface concentration of active sites for MSR and WGS reactions (mol/m^2)
CS_2^T, CS_{2A}^T	Total surface concentration of active sites for MD reaction (mol/m^2)
D_i	Diffusion coefficient of species i (m^2/s)
F	Faraday constant (96,485 C/eq)
h	Specific enthalpy (J/kg)
i	Fuel cell current density (A/cm^2)
K_V	Permeability of catalyst bed ($1.0 \times 10^{-9} m^2$)
K_i	Equilibrium constant for reaction i
k_i	Rate constant of reaction i ($m^2/mol\ s$)
LHV	Lower heating value (MJ/kg)
M_i	Molecular weight of species i ($kg/kmols$)
$\dot{m}_i$	Mass flow rate of species i (kg/s)
n	Number of cells in the fuel cell stack
$\dot{n}_i$	Molar flow rate of species i ($kmol/s$)
p	Pressure (Pa)
p_i	Partial pressure of species i (bar)
Pe	Electrical power provided by the fuel cell stack (3000 W)
$\dot{Q}$	Source term for energy equation (W/m^3)
$\dot{q}$	Wall heat flux (W/m^2)
R	Universal gas constant ($8314\ J/kmol\ K$)
$\dot{r}_j$	Rate of reaction j ($mol/m^2 s$)
S/M	Steam to methanol molar ratio at reformer inlet
T	Absolute temperature (K)
$\overline{U}$	Velocity vector (m/s)
V_{cat}	Volume of the active catalyst bed (m^3)
$V/cell$	Voltage delivered by a single cell in the fuel cell stack (V)
$W/F_{CH_3OH,in}$	Inverse molar flow rate of methanol at inlet per weight of catalyst ($kg\ s/mol$)
x_i	Molar fraction of component i
y_i	Mass fraction of component i

Greek symbols

ε_V	Volume porosity of the catalyst bed (0.36)
ε	Area porosity of the catalyst bed (0.36)
ζ	Methanol conversion rate
η	Reformer thermal efficiency (%)
λ	Thermal conductivity ($W/m\ K$)
λ_i	Stoichiometric ratio of component i in electrochemical reaction (1.2 for hydrogen, 2.0 for air)
μ	Dynamic viscosity ($kg/m\ s$)
$\dot{\omega}_i$	Source term for species i ($g/m^3 s$)
ρ	Density (kg/m^3)
Φ	Relative humidity of the reformate gas (%)
Φ_W	Parameter relating the gas composition to the WGS equilibrium

Subscripts

MD	Methanol decomposition reaction
MSR	Methanol steam reforming reaction
WGS	Water gas shift reaction
in	Property at reformer inlet
out	Property at reformer outlet
eq	Equivalent property
mix	Property of the gas mixture
cat	Catalyst

Introduction

There is a need to demonstrate power systems with a high fuel-to-electricity conversion efficiency used to extend the endurance of autonomous terrestrial vehicles and unmanned aerial vehicles (UAV) [1–3]. Fuel cells are energy conversion devices that convert the chemical energy of hydrogen directly to electricity at higher conversion efficiencies than other systems. Proton Exchange Membrane Fuel Cells (PEMFCs) deliver high-power density and offer the advantages of low weight and volume, rapid start-up, and better durability compared with other fuel cells, features that make them particularly suitable for automotive, underwater and aerial applications. High-Temperature PEMFCs (HT-PEMFCs) are capable of operating between 120 °C and 180 °C without external humidification, which renders them significant benefits over the low-temperature PEMFCs. These benefits include simplified water and thermal management, faster electrode kinetics for both electrode reactions, and an improved anode tolerance to carbon monoxide concentrations up to 3% [4], compared to less than 100 ppm in low-temperature PEMFCs. These benefits make HT-PEMFCs particularly suitable for reformate gas-operating automotive systems with a simplified design, in which the preferential oxidation stage in the fuel processing line can be eliminated. Also, they result in fuel cell power systems with a significant reduction in cost and complexity resulting from a smaller radiator in the cooling loop and the elimination of the humidifiers in the gas feed loops. In addition to these advantages, HT-PEMFCs offer the ability to use the fuel cell stack waste heat to boil water or heat space when used as a combined heat and power (CHP) system, increasing thus the system efficiency substantially when compared to conventional low temperature fuel cells power systems.

Even though hydrogen gas has the highest heat of combustion (MJ/kg), its energy density (MJ/m^3) is lower compared to other fuels. Despite having a higher energy conversion efficiency than other systems, a long-endurance automotive fuel cell power system using compressed hydrogen gas would

result in a system having a substantial volume due to the size of the gas cylinders. However, methanol is an energy carrier with energy density seven times higher than that of compressed hydrogen gas available using today's technology. Methanol steam reformers convert methanol solution into a hydrogen rich gas that contains as well carbon monoxide, carbon dioxide and traces of unused water and methanol vapors in a catalytic reaction at temperatures as low as 200 °C–350 °C and using inexpensive copper-based catalysts [5]. The reforming reaction is endothermic and requires the input of heat to sustain the process. This heat can be produced using the catalytic combustion of methanol vapor in excess of air in a Pt-based catalyst. The entire combustion/reforming of methanol can be obtained onboard and therefore can be integrated in the same power system with the fuel cell. Liquid methanol can be easily stored and carried onboard without requiring special technologies. The exhaust hot combustion gases and the reformate gas can be used to evaporate the methanol solution before entering the reformer reactor. Since the reforming process takes place at temperatures only slightly higher than the fuel cell operating temperature, the exhaust gases from the reformer may be used to preheat the fuel cell for a faster startup. HT-PEMFC fed with hydrogen from a methanol reformer would constitute a DC power system with high energy conversion efficiency and simplified thermal management that has not received sufficient attention in the past.

While HT-PEMFCs are tolerant to carbon monoxide in concentrations up to 3%, there is a penalty in their performance resulting from the dilution of hydrogen in the reformate gas. Hydrogen can be separated from the reformate gas before entering the fuel cell using an electrochemical hydrogen pump, which is essentially a PEMFC operating in reverse.

Since the reactions in a methanol steam reformer are overall endothermic and the catalyst particles have a relatively low thermal conductivity, the process in a fixed-bed steam reformer is characterized by a non-uniform temperature field which contains a cold region in its core where the methanol conversion efficiency is lower. To improve the methanol conversion efficiency through better thermal management, one uses a system of micro-channels machined in a highly thermally conductive material. Two methanol reformer designs with micro-channels have been studied: with parallel channels fabricated in a flat plate [6–12], or with a bundle of tubular channels fabricated in a cylindrical body [13,14]. The second design which was adopted in this work offers better technical solutions for maintaining the catalyst particles within the reformer channels.

The three overall reactions that occur in a methanol steam reformer are the methanol steam reforming (MSR) reaction (1), the water gas shift (WGS) reaction (2) and the methanol decomposition (MD) reaction (3):

$$CH_3OH + H_2O \leftrightarrow CO_2 + 3H_2 \qquad \left(\Delta_r H^0_{298}\right)_{MSR} = 49,500\, J/mol \tag{1}$$

$$CO + H_2O \leftrightarrow H_2 + CO_2 \qquad \left(\Delta_r H^0_{298}\right)_{WGS} = -41,100\, J/mol \tag{2}$$

$$CH_3OH \leftrightarrow 2H_2 + CO \qquad \left(\Delta_r H^0_{298}\right)_{MD} = 90,600\, J/mol \tag{3}$$

It can be noted that only two of these reactions are linearly independent and any one of them can be expressed as the algebraic sum of the other two. Because of this, there has been disagreement in the past regarding the reactions that must be included in a kinetic model of the process of methanol steam reforming on $Cu/ZnO/Al_2O_3$ catalyst. Previous numerical models have used one or two of the three possible reactions [7,8,13–17] and have considered that the other reactions were either at equilibrium, or that their reaction rates were negligible. Peppley [18] and Peppley et al. [19,20] have shown that the rate expressions for all three reactions (1–3) must be included in the kinetic model to accurately predict the composition of the product gas and that reaction models which involve only one or two of the possible three reactions are unable to explain the experimentally observed variation in the product composition. Furthermore, they showed that the MD reaction (3) occurs on a different type of catalyst sites than the other two reactions. The three - equation kinetic model of Peppley [18] and Peppley et al. [19,20] has been used in the past in Computational Fluid Dynamics (CFD) studies of methanol steam reformers [6,11,12,21–26]. Other three - equation kinetic models have been used in Ref. [27,28]. The interested reader may find other methanol reforming technologies for production of hydrogen in Ref. [29–34].

The objective of this study is to develop and use a CFD model of a methanol steam reformer to calculate the optimum operating regime and to size and optimize the design of a fuel processor for on-board production of hydrogen as fuel for a 3 kW HT-PEMFC power system. This endeavor represents an initial step in the fabrication of a power system with a high fuel-to-electricity conversion efficiency used to extend the endurance of autonomous terrestrial vehicles and unmanned aerial vehicles (UAVs).

The reminder of this paper is organized as follows: Section Mathematical model presents the CFD model used in this study. Section Model Validation compares numerical simulations obtained in this work to experimental results presented by Peppley [18] in order to calibrate and validate the numerical model. In Section Results and Discussion we perform numerical simulations and based on these calculations and on the operating constraints of high-temperature membrane electrode assemblies (MEAs), we select optimum operating regimes. In Section Reformer Design and Sizing we size the fuel processor based on the numerical results and optimize its design.

Mathematical model

The mathematical model used in the present analysis uses a three reaction model that accounts for methanol steam reforming (1), water gas shift (2) and methanol decomposition (3) reactions over a $Cu/ZnO/Al_2O_3$ catalyst. The 3D computational domain consists of a single cylindrical channel filled with active catalyst and having entry and exit regions filled with inert particles. A mixture of water and methanol vapor enters the flow domain through inlet. The domain is heated uniformly through the surrounding walls.

Conservation equations

The CFD model consists of the following governing equations:

The mass conservation equation:

$$\frac{\partial}{\partial t}(\varepsilon_V \rho) + \nabla \cdot (\varepsilon \rho \overline{U}) = 0 \tag{4}$$

The momentum conservation equations:

$$\frac{\partial}{\partial t}(\varepsilon_V \rho \overline{U}) = -\varepsilon_V \nabla p + \varepsilon_V \frac{\mu}{K_V} \overline{U} \tag{5}$$

The species conservation equations:

$$\frac{\partial}{\partial t}(\varepsilon_V \rho y_i) + \nabla \cdot (\varepsilon \rho \overline{U} y_i) - \nabla \cdot (\varepsilon \rho D_i \nabla y_i) = \varepsilon_V \dot{\omega}_i \qquad i = CH_3OH,\ H_2O,\ H_2,\ CO_2,\ CO \tag{6}$$

The energy conservation equation:

$$\frac{\partial}{\partial t}(\varepsilon_V \rho c_p T) + \nabla \cdot (\varepsilon \rho \overline{U} c_p T) - \nabla \cdot (\varepsilon \lambda_{eq} \nabla T) = \varepsilon_V \dot{Q} \tag{7}$$

Reaction kinetics model

In this study we used the reaction kinetics model of Peppley [18] and Peppley et al. [19,20] which consists of reversible Langmuir-Hinshelwood reaction rate expressions for each of the reactions (1–3) involved in the process of methanol steam reforming over Cu/ZnO/Al_2O_3 catalyst:

$$\dot{r}_{MSR} = \frac{k_{MSR} \cdot C_1 \cdot \left(p_{CH_3OH} / p_{H_2}^{1/2}\right) \cdot \left[1 - \frac{1}{K_{MSR}} \cdot \left(\frac{p_{H_2}^3 \cdot p_{CO_2}}{p_{CH_3OH} \cdot p_{H_2O}}\right)\right] \cdot CS_1^T \cdot CS_{1A}^T}{\left(1 + C_1 \cdot \left(p_{CH_3OH} / p_{H_2}^{1/2}\right) + C_2 \cdot p_{CO_2} \cdot p_{H_2}^{1/2} + C_3 \left(p_{H_2O} / p_{H_2}^{1/2}\right)\right)\left(1 + \left(C_4 \cdot p_{H_2}\right)^{1/2}\right)} \tag{8}$$

$$\dot{r}_{WGS} = \frac{k_{WGS} \cdot C_3' \cdot p_{CO} \cdot \left(p_{H_2O} / p_{H_2}^{1/2}\right) \cdot \left[1 - \frac{1}{K_{WGS}} \cdot \left(\frac{p_{H_2} \cdot p_{CO_2}}{p_{CO} \cdot p_{H_2O}}\right)\right] \cdot \left(CS_1^T\right)^2}{\left(1 + C_1 \cdot \left(p_{CH_3OH} / p_{H_2}^{1/2}\right) + C_2 \cdot p_{CO_2} \cdot p_{H_2}^{1/2} + C_3 \cdot \left(p_{H_2O} / p_{H_2}^{1/2}\right)\right)^2} \tag{9}$$

$$\dot{r}_{MD} = \frac{k_{MD} \cdot C_5 \cdot \left(p_{CH_3OH} / p_{H_2}^{1/2}\right) \cdot \left[1 - \frac{1}{K_{MD}} \cdot \left(\frac{p_{H_2}^2 \cdot p_{CO}}{p_{CH_3OH}}\right)\right] \cdot CS_2^T \cdot CS_{2A}^T}{\left(1 + C_5 \cdot \left(p_{CH_3OH} / p_{H_2}^{1/2}\right) + C_6 \cdot \left(p_{H_2O} / p_{H_2}^{1/2}\right)\right)\left(1 + \left(C_7 \cdot p_{H_2}\right)^{1/2}\right)} \tag{10}$$

The expressions for the reaction kinetics parameters in Eq. 8–10 are shown in Table 1.

Constitutive relations

The sources for chemical species are calculated from the reaction rates (8–10):

$$\dot{\omega}_{CH_3OH} = (-\dot{r}_{MSR} - \dot{r}_{MD}) \cdot M_{CH_3OH} \cdot a_{ref} \tag{11}$$

$$\dot{\omega}_{H_2} = (3 \cdot \dot{r}_{MSR} + 2 \cdot \dot{r}_{MD} + \dot{r}_{WGS}) \cdot M_{H_2} \cdot a_{ref} \tag{12}$$

$$\dot{\omega}_{CO_2} = (\dot{r}_{MSR} + \dot{r}_{WGS}) \cdot M_{CO_2} \cdot a_{ref} \tag{13}$$

$$\dot{\omega}_{H_2O} = (-\dot{r}_{MSR} - \dot{r}_{WGS}) \cdot M_{H_2O} \cdot a_{ref} \tag{14}$$

$$\dot{\omega}_{CO} = (\dot{r}_{MD} - \dot{r}_{WGS}) \cdot M_{CO} \cdot a_{ref} \tag{15}$$

The heat source in the energy conservation Eq. (7) represents the heat of reactions:

$$\dot{Q} = -\left[\left(\Delta_r H_{298}^0\right)_{MSR} \cdot \dot{r}_{MSR} + \left(\Delta_r H_{298}^0\right)_{WGS} \cdot \dot{r}_{WGS} + \left(\Delta_r H_{298}^0\right)_{MD} \cdot \dot{r}_{MD}\right] \cdot a_{ref} \tag{16}$$

The thermodynamic properties μ, λ and c_p of the gas mixture are calculated as mass fraction weighted averages of the thermodynamic properties of gas species:

$$\Phi_{mix} = \sum_i y_i \cdot \Phi_i \qquad \Phi = \mu,\ \lambda,\ C_p \tag{17}$$

The expressions used in this study for the thermodynamic properties of the gas species as function of temperature are shown in Table 2. The density of the gas mixture is calculated as:

$$\rho = \frac{p}{RT \sum_i \frac{y_i}{M_i}} \tag{18}$$

The equivalent thermal conductivity of the porous catalyst region is the weighted average of the thermal conductivities of the gas mixture and of the solid matrix:

$$\lambda_{eq} = \varepsilon_V \lambda_{mix} + (1 - \varepsilon_V) \lambda_{cat} \tag{19}$$

The values of the physical properties of the catalyst are shown in Table 3.

The partial pressures in the expressions for the reaction rates (8–10) are calculated as a function of mass fractions as:

Table 1 – The parameters of the reaction kinetics model [18,20].

Parameter	Expression	Units
K_{MSR}	$exp\left(24.39-\frac{7,060}{T}\right)$	bar^2
K_{WGS}	$exp\left(-4.67+\frac{4,773}{T}\right)$	–
K_{MD}	$exp\left(29.06-\frac{11,833}{T}\right)$	bar^2
k_{MSR}	$7.4\times10^{14}exp\left(\frac{-102,800}{RT}\right)$	$m^2/mol\ s$
k_{WGS}	$5.9\times10^{13}exp\left(\frac{-87,600}{RT}\right)$	$m^2/mol\ s$
k_{MD}	$3.8\times10^{20}exp\left(\frac{-170,000}{RT}\right)$	$m^2/mol\ s$
C_1	$exp\left(\frac{-41.8}{R}+\frac{20,000}{RT}\right)$	$bar^{-0.5}$
C_2	$exp\left(\frac{179.2}{R}-\frac{100,000}{RT}\right)$	$bar^{-1.5}$
C_3	$exp\left(\frac{-44.58}{R}+\frac{20,000}{RT}\right)$	$bar^{-0.5}$
C_3'	$exp\left(\frac{-44.58}{R}+\frac{20,000}{RT}\right)$	$bar^{-1.5}$
C_4	$exp\left(\frac{-100.8}{R}+\frac{50,000}{RT}\right)$	bar^{-1}
C_5	$exp\left(\frac{30}{R}+\frac{20,000}{RT}\right)$	$bar^{-0.5}$
C_6	$exp\left(\frac{30}{R}+\frac{20,000}{RT}\right)$	$bar^{-0.5}$
C_7	$exp\left(\frac{-46.2}{R}+\frac{50,000}{RT}\right)$	bar^{-1}
CS_1^T	7.5×10^{-6}	mol/m^2
CS_{1A}^T	1.5×10^{-5}	mol/m^2
CS_2^T	7.5×10^{-6}	mol/m^2
CS_{2A}^T	1.5×10^{-5}	mol/m^2

Table 3 – Physical properties of the catalyst.

Property	Value
Density, $\rho_{cat}\cdot(kg/m^3)$	1220 (from Ref. [39])
Thermal conductivity, $\lambda_{cat}\cdot(W/m\,K)$	10
Volumetric porosity of catalyst bed, ε_V	0.36
Permeability of catalyst bed, $K_V\cdot(m^2)$	1.0×10^{-9}

$$p_i = px_i \times 10^{-5} \tag{20}$$

Boundary conditions

Inlet boundary conditions

The operation of catalytic reformers is usually analyzed as a function of two parameters at the reformer inlet: the inverse of molar flow rate of methanol per weight of catalyst, $W/F_{CH_3OH,in}$ and the steam-to-methanol (or to carbon) molar ratio, S/M. The latter is defined as:

$$S/M = \frac{\dot{n}_{H_2O}}{\dot{n}_{CH_3OH}} = \frac{\dot{m}_{H_2O}}{\dot{m}_{CH_3OH}}\cdot\frac{M_{CH_3OH}}{M_{H_2O}} \tag{21}$$

The boundary conditions at the reformer inlet are therefore specified as functions of $W/F_{CH_3OH,in}$ and S/M. For the momentum equations, the mass flow rate of methanol/water mixture at inlet is:

$$\dot{m}_{in} = \frac{(S/M\cdot M_{H_2O} + M_{CH_3OH})\cdot(1-\varepsilon_V)\cdot V_{cat}\cdot\rho_{cat}}{1000\cdot(W/F_{CH_3OH,in})} \tag{22}$$

The boundary condition for the species conservation equations are:

$$y_{CH_3OH,in} = \frac{1}{S/M\frac{M_{H_2O}}{M_{CH_3OH}}+1} \tag{23}$$

Table 2 – The thermodynamic properties of the gas species as function of absolute temperature [35–38].

Component	Property	Expression
CH_3OH	$c_p\ (J/kg\,K)$	$-0.001T^2+3.419T+400.99$
	$\mu\ (kg/m\,s)$	$[0.493\cdot\exp(0.0025\cdot T)]\times10^{-5}$
	$\lambda(W/m\,K)$	$1.034\times10^{-5}T-1.653\times10^{-3}$
	$LHV\cdot[MJ/kg]$	20.09
H_2O	$c_p\ (J/kg\,K)$	$-1.5071\times10^{-9}T^5+4.0048\times10^{-6}T^4-4.2374\times10^{-3}T^3+2.2340T^2-5.8718\times10^2T+6.3552\times10^4$
	$\mu\ (kg/m\,s)$	$(0.0036T-0.1016)\times10^{-5}$
	$\lambda\ (W/m\,K)$	$8.070\times10^{-5}T-6.269\times10^{-3}$
H_2	$c_p\ (J/kg\,K)$	$8.551\times10^{-6}T^3-1.363\times10^{-2}T^2+7.491T+1.311\times10^4$
	$\mu\ (kg/m\,s)$	$(0.0017T+0.4094)\times10^{-5}$
	$\lambda\ (W/m\,K)$	$0.0004T+0.0688$
	$LHV\cdot[MJ/kg]$	119.96
CO_2	$c_p\ (J/kg\,K)$	$331.33\times\ln(T)-1041.7$
	$\mu\ (kg/m\,s)$	$(0.0039T+0.3218)\times10^{-5}$
	$\lambda\ (W/m\,K)$	$8.001\times10^{-5}T-7.581\times10^{-3}$
CO	$c_p\ (J/kg\,K)$	$0.0003\times T^2-0.1002\times T+1041.7$
	$\mu\ (kg/m\,s)$	$(0.0034T+0.9092)\times10^{-5}$
	$\lambda\ (W/m\,K)$	$6.90\times10^{-5}T+4.50\times10^{-3}$

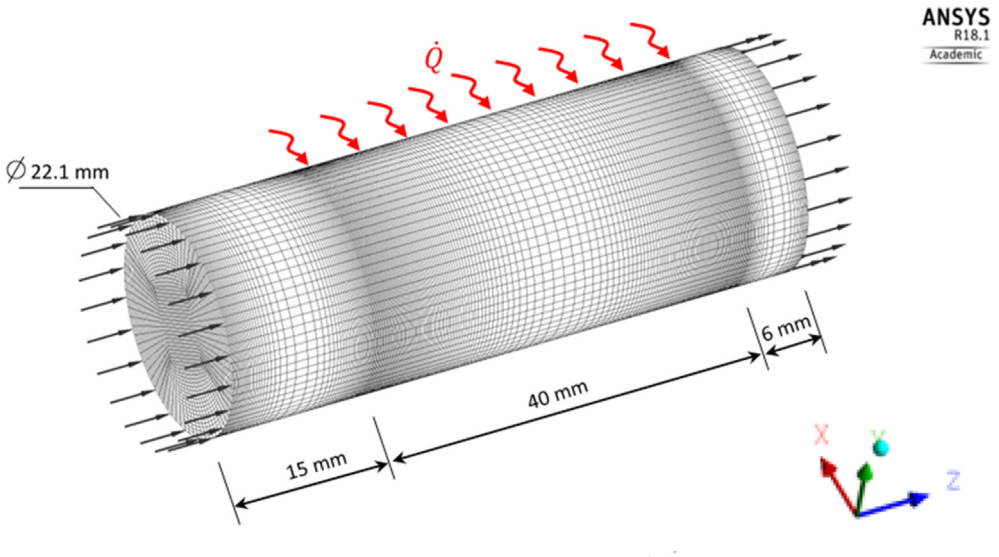

Fig. 1 – The computational domain for model validation.

$$y_{H_2O,in} = 1 - \frac{1}{S/M\frac{M_{H_2O}}{M_{CH_3H}} + 1} \quad (24)$$

$$y_{H_2,in} = y_{CO_2,in} = y_{CO,in} = 0 \quad (25)$$

The temperature of the reactant gasses at inlet is known.

Wall boundary conditions

The walls bounding the channels are impermeable to gasses but are thermally conductive. The gas velocities and species fluxes are set to zero. The walls bounding the chemically inactive entry and exit regions of the domain are adiabatic (see Fig. 1). The heat flux at the wall bounding the active catalyst region is assigned as:

$$\dot{q} = \frac{\int \dot{Q} dV}{area_{heating\ wall}} \quad (26)$$

In Eq. (26) the integral at the numerator is calculated over the volume occupied by the active catalyst region, V_{cat}. Since the reaction is endothermic and the specific heat, c_p of the

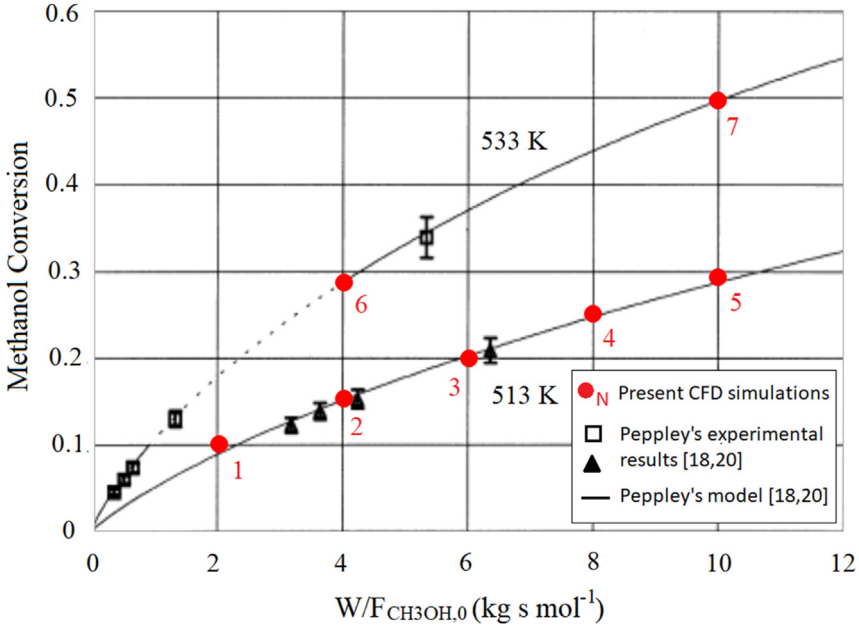

Fig. 2 – Present CFD model prediction vs experimental results of Peppley [18,20] at 1 atm and S/M = 1. The results of the present model are plotted over the original graph in Ref. [20] (reprinted with permission from Elsevier).

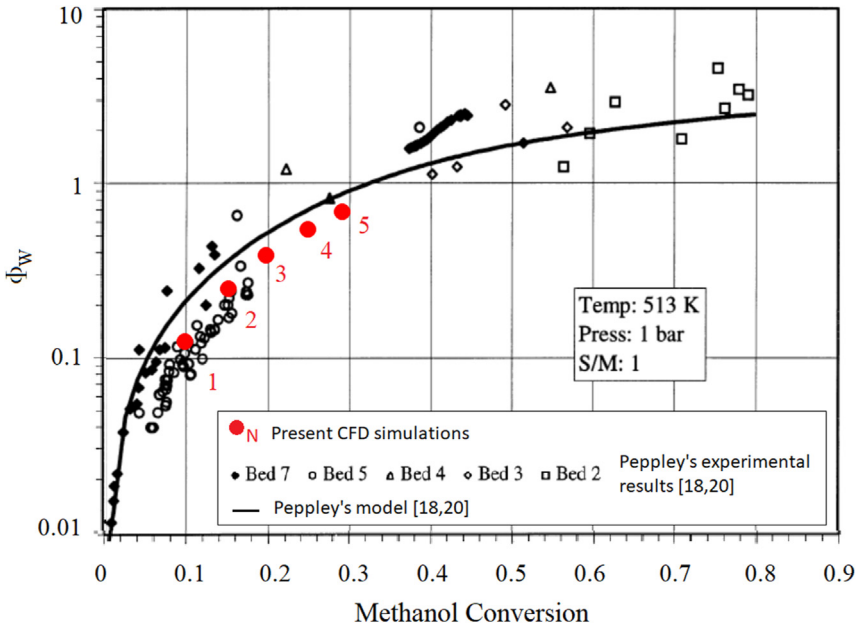

Fig. 3 – Present CFD model prediction vs experimental results of Peppley [18,20] The results of the present model are plotted over the original graph in Ref. [20] (reprinted with permission from Elsevier).

Table 4 – Simulation results for model validation.

Case #	Operating Parameters				Mass flow rates of reformate components at exit (g/s) x 10^{-3}						
	T_{in} (K)	p (atm)	S/C	W/$F_{CH3OH,in}$ (kg s mol^{-1})	$\dot{m}_{H_2}$	$\dot{m}_{CO_2}$	$\dot{m}_{CO}$	$\dot{m}_{CH_3OH}$	$\dot{m}_{H_2O}$	ζ	φ_W
1	513	1	1	2	3.46	26.32	0.140	172.30	96.91	0.100	0.23
2	513	1	1	4	2.59	20.22	0.084	81.06	45.60	0.153	0.47
3	513	1	1	6	2.2	17.59	0.057	51.10	28.75	0.199	0.75
4	513	1	1	8	2.02	16.59	0.062	20.20	35.91	0.250	1.05
5	513	1	1	10	1.85	15.56	0.058	27.11	15.24	0.292	1.24
6	533	1	1	4	4.52	37.87	0.355	68.36	38.46	0.286	0.411
7	533	1	1	10	3.39	25.67	0.624	19.28	10.85	0.496	0.92

reaction products are higher than that of the reactants, the integrant at the numerator, expression (16) decreases as the reaction advances in time until it reaches an equilibrium value. If the boundary condition (26) would be allowed to follow the heat of reaction, $\dot{Q}$, the reaction would eventually seize. The integrant is therefore kept constant in time and is calculated from (16) for fresh reactant composition at the operating temperature.

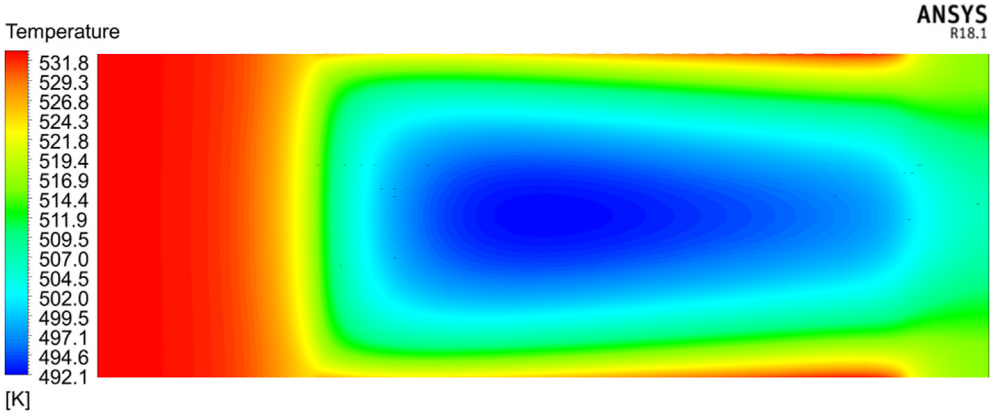

Fig. 4 – Temperature distribution along the reformer, from inlet to outlet, at 533 K, 1 atm, S/M = 1 and.$W/F_{CH_3OH,in}$ = 4.

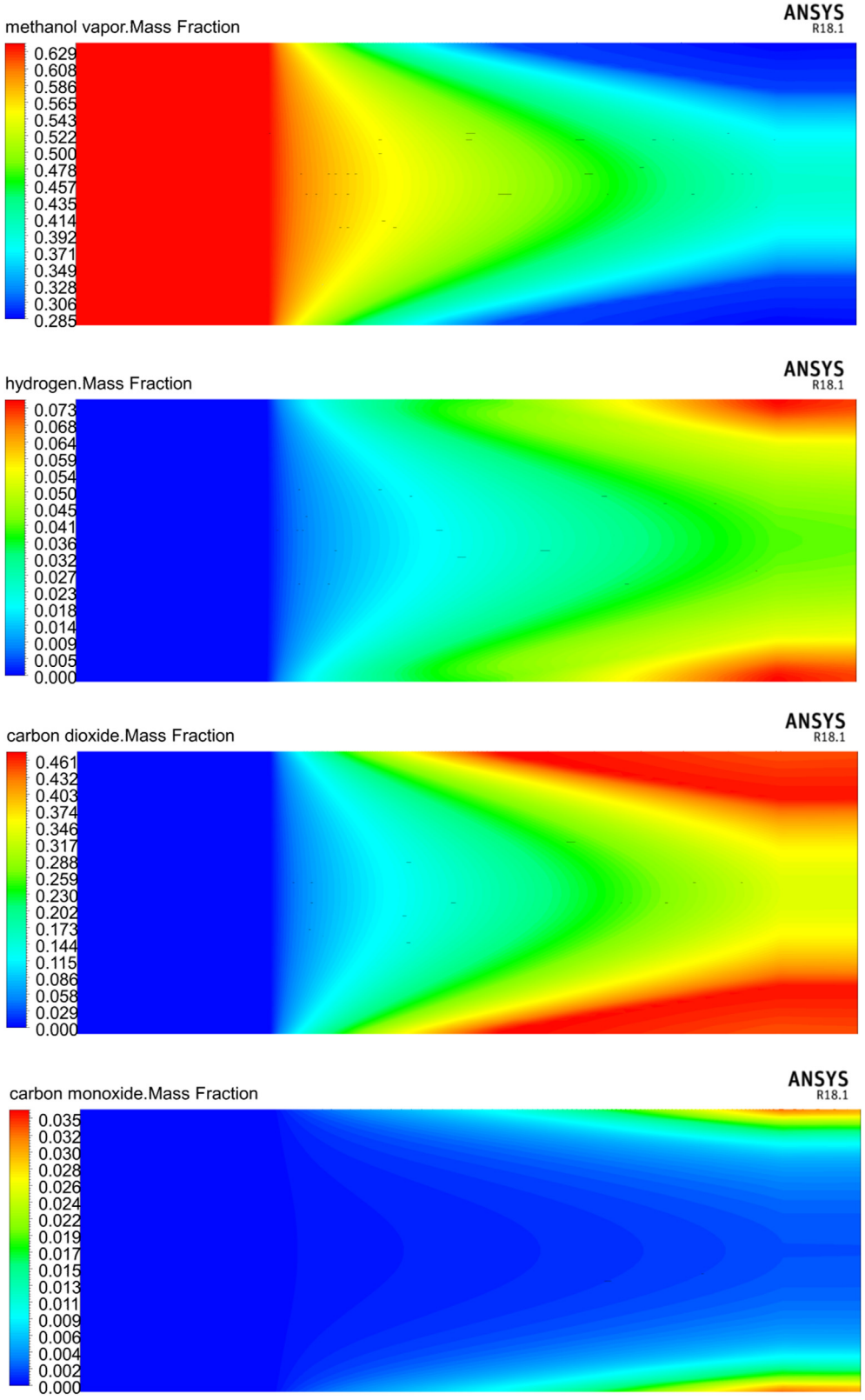

Fig. 5 – Mass fraction distributions of (a) methanol, (b) hydrogen, (c) carbon dioxide and (d) carbon monoxide, at 533 K, 1 atm, $S/M = 1$ and $W/F_{CH_3OH,in} = 10$.

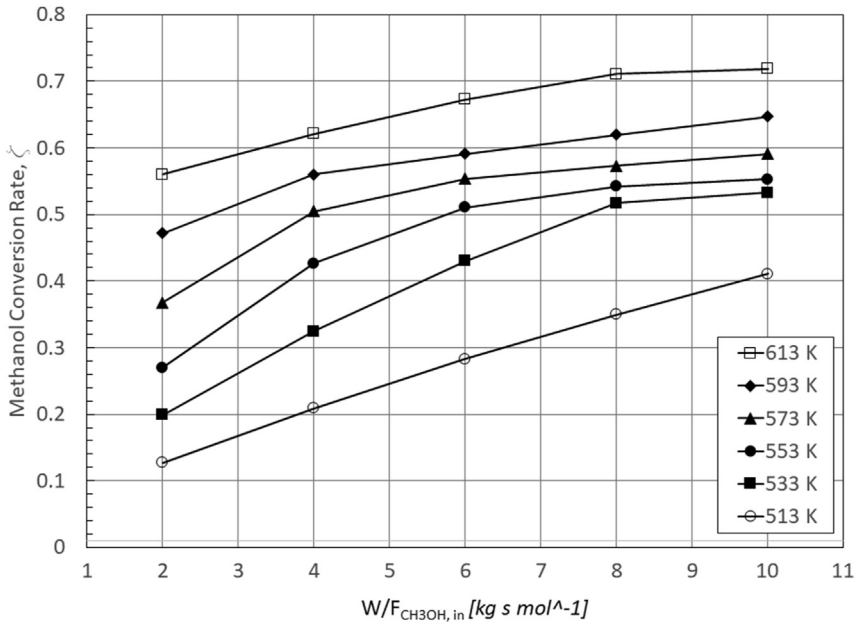

Fig. 6 – Methanol conversion rate as function of temperature and $W/F_{CH_3OH,in}$.

Parameters describing the reformer performance

The methanol conversion rate and the reformer thermal efficiency are defined as:

$$\zeta = \frac{\dot{n}_{CH_3OH,in} - \dot{n}_{CH_3OH,out}}{\dot{n}_{CH_3OH,in}} \tag{27}$$

and

$$\eta = \frac{LHV_{H_2} \cdot \dot{m}_{H_2,out}}{LHV_{CH_3OH} \cdot (\dot{m}_{CH_3OH,in} - \dot{m}_{CH_3OH,out}) + \dot{q} \cdot area_{heating\ wall}} \times 100 \tag{28}$$

By convention, in this study the reformer operating temperature was considered to be the average temperature over the active catalyst region:

$$T = \frac{1}{\dot{m}} \int_{active\ region} T d\dot{m} \tag{29}$$

Model validation

The CFD calculations were performed using ANSYS-CFX software with its High-Resolution Advection Scheme. The

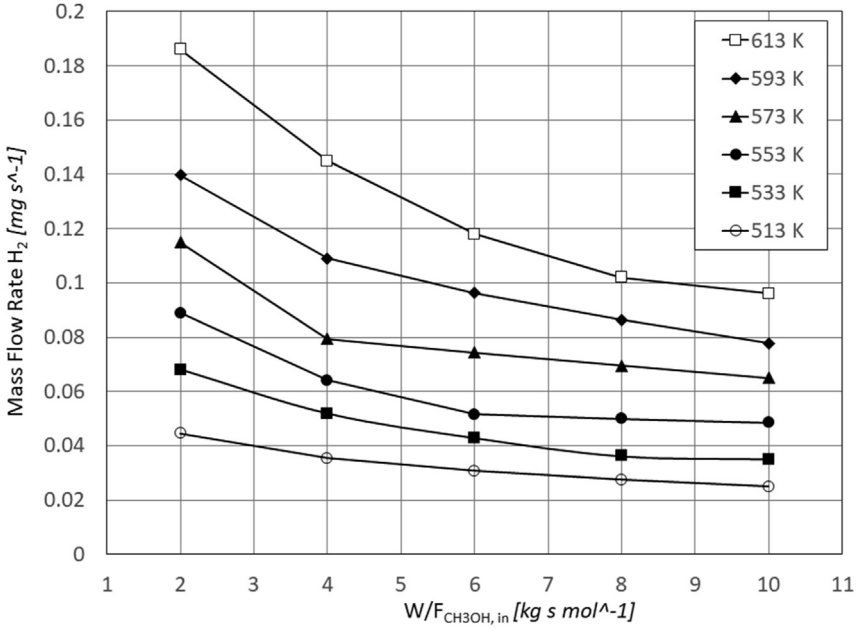

Fig. 7 – Mass flow rate of hydrogen produced as function of temperature and $W/F_{CH_3OH,in}$.

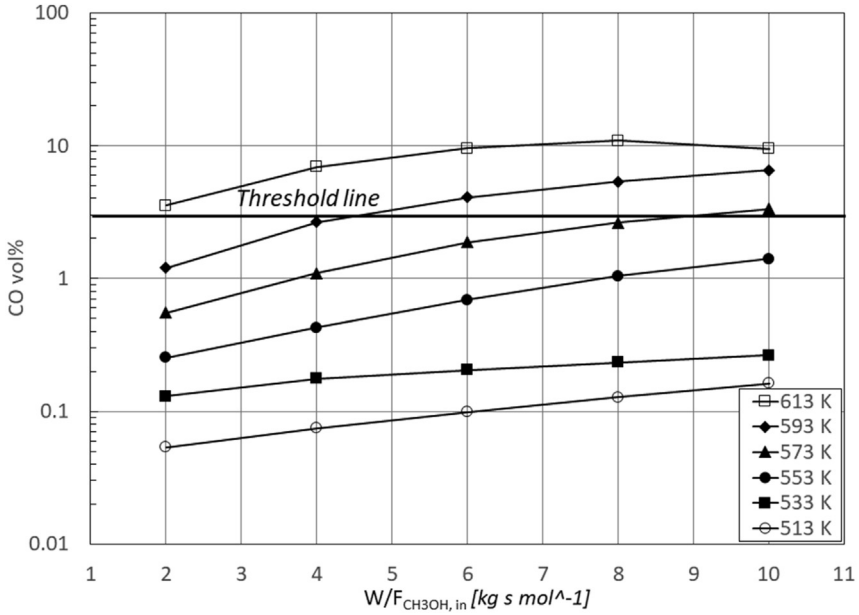

Fig. 8 – CO vol% in reformate gas as function of temperature and $W/F_{CH_3OH,in}$.

domain grid (Fig. 1) was generated using ICEM CFD software and consists of 392,000 hexahedral elements with a maximum length ratio of 7.9. The CFD model was validated against the experimental results of Peppley [18,20]. The computational domain (Fig. 1) corresponds to Peppley's experimental setup [18] and consists of a tubular fixed-bed reactor having a 22.1 mm internal diameter, a 15 mm long non-reacting entry section filled with inert particles, a 40 mm long reactive section filled with $Cu/ZnO/Al_2O_3$ catalyst particles, followed by a 6 mm long non-reacting exit section filled with inert particles. The active region of the reformer is heated, while the inert entry and exit sections have adiabatic walls. The temperature of the methanol solution at the reformer inlet was set equal to the operating reformer temperature.

Simulations were run for operating temperatures of 513K and 533K, for an operating pressure of 1 atm, for a steam to methanol molar ratio, S/M of 1 and for different values of $W/F_{CH_3OH,in}$. Figs. 2 and 3 show an excellent agreement between our simulations (numbered large red circles) and Peppley's experimental results [18,20] for a wide range of operating conditions. The curves in Figs. 2 and 3 represent the prediction of Peppley's model. The numbers correspond to the

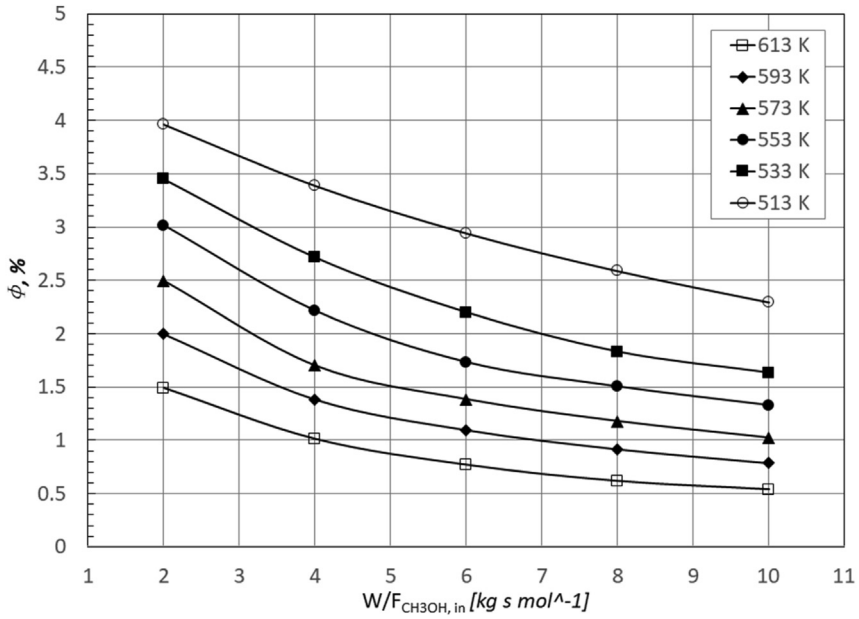

Fig. 9 – Relative humidity of the reformate gas after cooling to a fuel cell operating temperature of 180 °C.

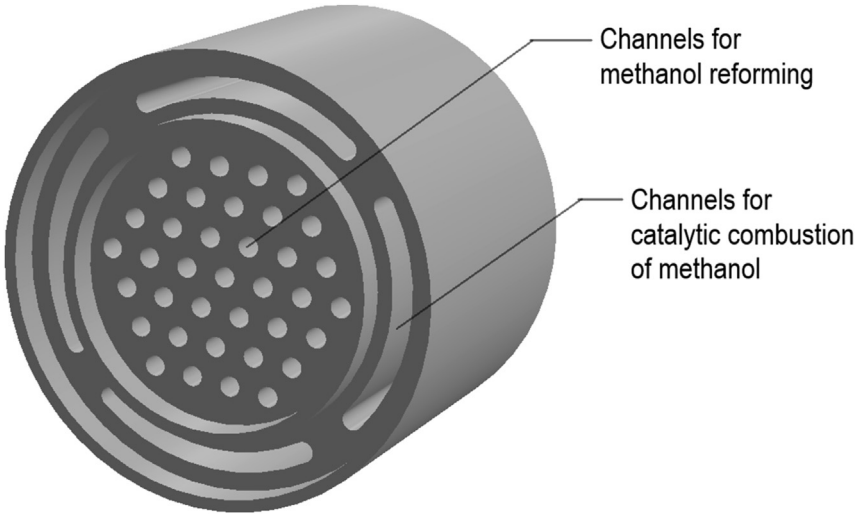

Fig. 10 – Design of a single methanol reforming unit.

cases shown in Table 4. Fig. 3 represents the gas composition relative to the water gas shift reaction as a function of methanol conversion. Parameter φ_W in Fig. 3 defined as:

$$\varphi_W = \frac{P_{CO_2} P_{H_2}}{P_{CO} P_{H_2O}} \frac{1}{K_{WGS}} \tag{30}$$

is a measure of the product composition relative to the water gas shift reaction (when the WGS reaction is at equilibrium $\varphi_W = 1$). In our calculations, the partial pressures of the gas species were calculated at reformer outlet and the equilibrium constant was calculated at the reformer operating temperature.

Fig. 4 presents the temperature field along the reformer from inlet to outlet, at an operating temperature of 533 K, 1 atm, S/M = 1 and $W/F_{CH_3OH,in} = 4$ (case 6 in Table 4). Since the overall reaction in the reformer is endothermic and the thermal conductivity of the catalyst is relatively low, the temperature distribution is characterized by a colder region in the reformer core, about 40 K below the temperature in the regions close to the heating walls. In this colder region the reaction rates are lower and therefore the methanol conversion efficiency is lower. This expected result which is characteristic to fixed-bed catalytic reactors points out their disadvantage and the need to use reformers with micro-channels fabricated in a material with high thermal conductivity.

Fig. 5 presents the mass fraction distributions of the reformate gas components along the reformer at an operating

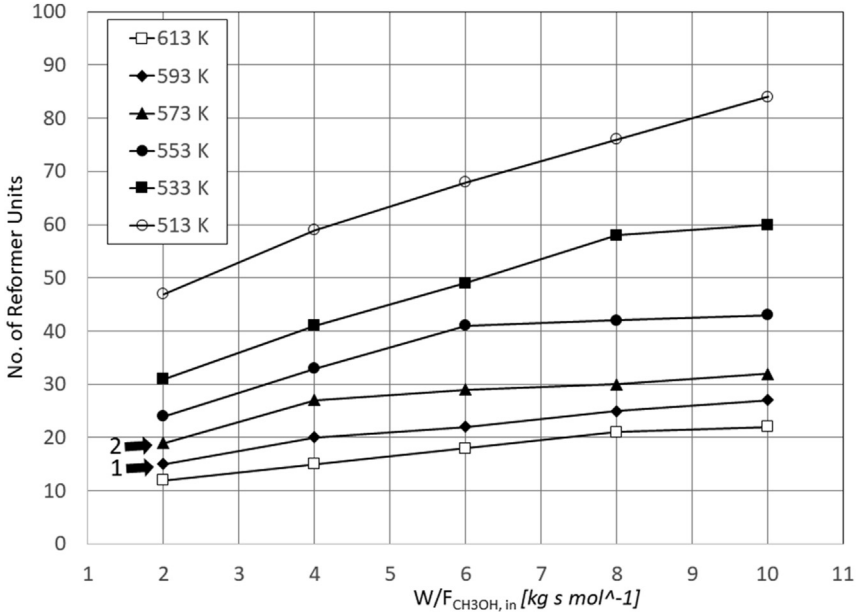

Fig. 11 – Number of reformer units required for each simulated case.

Table 5 – Reformer size, consumption of methanol solution, reformate gas composition and quality and reformer performance parameters for the operating regimes selected in Fig. 11.

Operating regime	# of reformer units	Consumption methanol solution (g/s)	Mass flow rates of reformate components at exit (g/s)					Reformate quality		Reformer Performance	
			$\dot{m}_{H_2}$	$\dot{m}_{CO_2}$	$\dot{m}_{CO}$	$\dot{m}_{CH_3OH}$	$\dot{m}_{H_2O}$	CO vol%	Relative humidity	ζ	φ_W
1	15	1.686	0.077	0.688	0.030	0.570	0.321	1.20%	2.0%	0.472	66.8%
2	19	2.049	0.077	0.660	0.016	0.829	0.467	0.55%	2.5%	0.368	73.9%

temperature of 533 K, 1 atm, S/M = 1 and $W/F_{CH_3OH,in} = 10$ (case 7 in Table 4).

Results and discussion

The methanol reformer design adopted in this work consists of a bundle of 2 mm diameter, equally distanced tubular channels fabricated in a cylindrical body. This design offers a better thermal management and therefore higher methanol conversion efficiency when compared to fixed-bed reactors. The computational domain used in the analysis consists of a single 2 mm diameter, 60 mm long channel comprising a 5 mm long non-reacting entry region filled with inert particles, a 50 mm long reactive region filled with catalyst and a 5 mm long non-reacting exit region filled with inert particles.

Numerical simulations were performed for six different operating temperatures and five different molar flow rates of methanol per weight of catalyst, $W/F_{CH_3OH,in}$ at the reformer inlet. In all cases, the operating pressure was 1 atm and the steam-to-methanol molar ratio, S/M = 1. Higher ratios were not considered in the analyses as it would have resulted in unacceptable values of the reformate gas relative humidity. The numerical results were used to select the optimum reformer operating regime and determine the process parameters. The optimum operating regime is selected as a compromise between high methanol conversion rate, high hydrogen production and for a reformate gas composition that can be tolerated by HT-PEM MEAs. *Advent TPS®* are PA–doped HT-PEM MEAs that can operate between 120 °C to 200 °C and can tolerate CO concentrations in the reformate gas up to 3%. However, the amount of water vapor in the anode and cathode reactant gasses must be minimized to prevent the leach of PA out of the MEA and reduce their proton conductivity.

Fig. 6 through 9 are plots of the methanol conversion rate (ζ), of the hydrogen produced - $\dot{m}_{H_2} \cdot (mg/s)$, of the CO vol% in the reformate gas and of the reformate gas relative humidity (φ), all as function of reformate operating temperature and $W/F_{CH_3OH,in}$.

Higher methanol conversion rates (Fig. 6) and hydrogen yields (Fig. 7) are obtained at higher operating temperatures. The reformer operating regime will therefore be sought at the highest practical operating temperature.

However, as shown in Fig. 8, the CO vol% in the reformate gas increases as well with temperature. Since commercial HT-PEM MEAs have a CO tolerance up to 3%, only the operating regimes in Fig. 8 situated below the threshold line are acceptable.

Before delivering it to the fuel cell, the reformate gas must be cooled to the fuel cell operating temperature. Fig. 9 shows the relative humidity of the reformate gas calculated using the Antoine equation for a fuel cell operating temperature of 180 °C as:

$$\varphi = \frac{x_{H_2O} \cdot p}{10^{\left(8.14019 - \frac{1810.94}{244.485 + 180}\right) \cdot 0.00131579}} \tag{31}$$

For all simulated operating regimes, the relative humidity of the reformate gas is below 5%, which is acceptable by PA-doped HT-PEM MEAs. We note that operating regimes

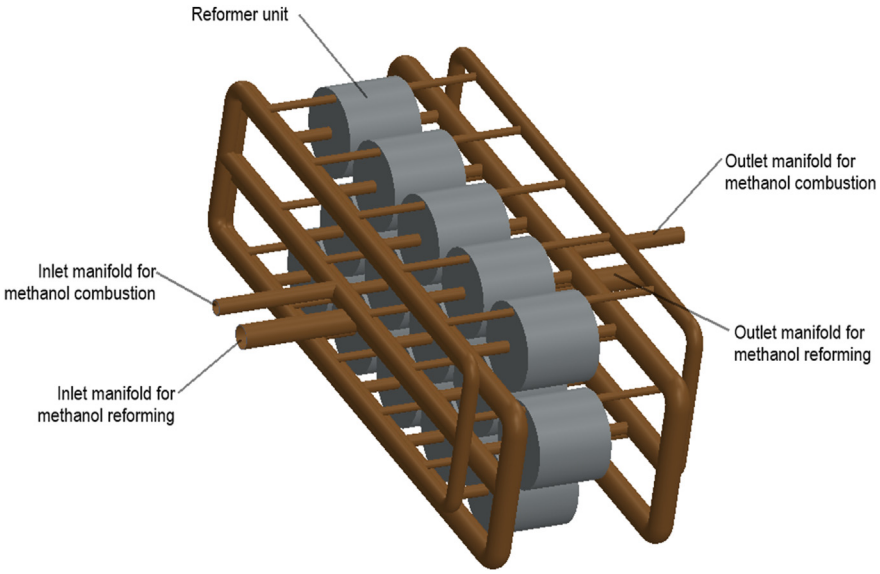

Fig. 12 – Methanol reformer consisting of 15 reformer units for on-board production of hydrogen as fuel for a 3 kW HT-PEMFC power system.

corresponding to higher operating temperatures result in lower relative humidity of the reformate gas.

Reformer design and sizing

The reformer must produce sufficient hydrogen to operate a 3 kW HT-PEMFC. The fuel cell stack sought to be used in the power system is based on 166.25 cm^2 active area *Advent TPS®* MEAs which can deliver a current density of 0.8 A/cm^2 at 0.5 V/cell when operated with hydrogen and air at 1.2 and 2.0 stoichiometric ratios at 180°C [40]. The number of cells in the fuel cell stack is calculate as:

$$n = \frac{P_e}{i \cdot V/cell \cdot A} \tag{32}$$

The number of cells in the fuel cell stack - 46 as provided by Eq. (32) is rounded up to the nearest integer. The mass flow rate of hydrogen *(g/s)* required to operate the fuel cell stack is calculated based on Faraday's law:

$$\dot{m}_{H_2} = \lambda_{H_2} \cdot \frac{i \cdot A}{2F} \cdot n \cdot M_{H_2} \tag{33}$$

which for a hydrogen stoichiometric ratio - $\lambda_{H_2} = 1.2$ results in 0.077 g/s of hydrogen.

The reformer design for the 3 kW power system comprises of a number of reactor units, each consisting of a bundle of 37 equally spaced, 50 mm long and 2 mm in diameter channels (see Section Results and Discussion) fabricated in a high-temperature conductive cylindrical body and filled with $Cu/ZnO/Al_2O_3$ catalyst particles for methanol reforming. They are surrounded by four peripheral channels filled with catalyst for the catalytic combustion of methanol which provides heat to support the endothermic reforming reaction of methanol (Fig. 10).

The number of reforming units for each case simulated in Section Results and Discussion is determined by dividing the mass flow rate of hydrogen required to operate the fuel cell stack (0.077 g/s) by the mass flow rate of hydrogen produced (Fig. 7) and is shown in Fig. 11.

Two operating regimes that result in a practical reformer volume (points 1 and 2 in Fig. 11) are selected and the reformate gas composition, the methanol consumption rate, the methanol conversion rate and the thermal efficiency of the reformer are compared (Table 5). Note that all operating regimes corresponding to 613 K and most regimes corresponding to 593 K are not considered since their CO volume % is higher than the 3% threshold (Fig. 8) acceptable by PA-doped HT-PEM MEAs. All other operating regimes corresponding to lower reformer operating temperature are disregarded as they result in an unpractical reformer size.

It is noted from Table 5 that operating regime 1 ($T = 593\ K$ and $W/F_{CH_3OH,in} = 2$) results in a smaller reformer size (15 units), lower methanol consumption, better methanol conversion rate (ζ), lower reformate relative humidity, but higher CO volume % and lower reformer thermal efficiency (η) than operating regime 2 ($T = 573$ K and $W/F_{CH_3OH,in} = 2$). While in both cases the reformate gas quality (CO vol% and relative humidity) are acceptable for operation with PA-doped HT-PEM MEAs, the methanol consumption rate and the reformer thermal efficiency have different impacts on the overall fuel cell power system efficiency. Both cases are retained for a further analysis of the fuel cell power system efficiency.

Fig. 12 shows the design of the methanol reformer consisting of 15 reformer units for on-board production of hydrogen as fuel for a 3 kW HT-PEMFC power system.

Conclusions

We present a Computational Fluid Dynamics model to determine the optimum operating regime and the process parameters of a methanol reformer for on-board production of

hydrogen as fuel for a 3 kW HT-PEMFC power system. The analysis uses a three reactions model for methanol steam reforming, water gas shift and methanol decomposition reactions on $Cu/ZnO/Al_2O_3$ catalyst. Numerical simulations are performed at single channel level for a range of reformer operating temperatures and values of the molar flow rate of methanol per weight of catalyst at the reformer inlet. Based on the numerical simulations results, the reactor is sized and its design is optimized. Two operating regimes of the fuel processor are selected which offer high methanol conversion rate and high hydrogen production while simultaneously result in a small reformer size and a reformate gas composition that can be tolerated by PA-doped HT-MEAs for PEMFCs.

The first selected operating regime results in a smaller reformer size (15 units), lower consumption of methanol, better methanol conversion rate, lower reformate relative humidity, but higher CO volume % and lower reformer thermal efficiency than the second selected operating regime. While in both cases the reformate gas quality (CO vol% and relative humidity) are acceptable for operation with PA-doped HT-PEM MEAs, the methanol consumption and the reformer thermal efficiency have different impacts on the overall power system efficiency. Both cases are retained for a further efficiency analysis of the overall fuel cell power system.

Funding

This work was supported in part by the National Institute of Food and Agriculture/United States Department of Agriculture [grant number 2019-33610-29797].

Declaration of competing interest

The authors declare that they have no known competing financial interests or personal relationships that could have appeared to influence the work reported in this paper.

REFERENCES

[1] Ratcliffe J. Net efficiency concepts in small UAS propulsion systems. In: Advances in unmanned system propulsion, technical webinar series from the editors of SAE (SAE webminar); 2017. June 27.
[2] Swider-Lyons K. Hydrogen fuel cells for UAVs. In: Advances in unmanned system propulsion, technical webinar series from the editors of SAE (SAE webminar); 2017. June 27.
[3] Ransom D. Benefiting government, industry and the public through innovative science and technology. In: Advances in unmanned system propulsion, technical webinar series from the editors of SAE (SAE webminar); 2017. June 27.
[4] Schmidt TJ. High-temperature polymer electrolyte fuel cells: durability insights. In: Buchi FN, Inaba M, Schmidt TJ, editors. Polymer electrolyte fuel cell durability. New York: Springer Science + Business Media, LLC; 2009. p. 199–201. https://doi.org/10.1007/978-0-387-85536-3_9.
[5] de Wild PJ, Verhaak MJFM. Catalytic production of hydrogen from methanol. Catalysis Today 2010;60:3–10. https://doi.org/10.1016/S0920-5861(00)00311-4.
[6] Hsueh CY, Chu HS, Yan WM, Chen CH. Numerical study of heat and mass transfer in a plate methanol steam micro reformer with methanol catalytic combustor. Int J Hydrogen Energy 2010;35:6227–38. https://doi.org/10.1016/j.ijhydene.2010.03.036.
[7] Hao Y, Du X, Yang L, Shen Y, Yang Y. Numerical simulation of configuration and catalyst-layer effects on micro-channel steam reforming of methanol. Int J Hydrogen Energy 2011;36:15611–21. https://doi.org/10.1016/j.ijhydene.2011.09.038.
[8] Kim T. Micro power generation from micro fuel cell combined with micro methanol reformer. In: Micro electronic and mechanical systems. IntechOpen; 2009. p. 25–51. https://doi.org/10.5772/7002.
[9] Park DE, Kim T, Kwon S, Kim CK, Yoon E. Micromachined methanol steam reforming system as a hydrogen supplier for portable proton exchange membrane fuel cells. Sensor Actuator 2007;135:58–66. https://doi.org/10.1016/j.sna.2006.07.008.
[10] Jang JY, Cheng HC, Huang YX, Lee CI, Leu CH. Optimal design of parallel channel patterns in a micro methanol steam reformer. Int J Hydrogen Energy 2012;37:16974–85. https://doi.org/10.1016/j.ijhydene.2012.08.042.
[11] Tadbir MA, Akbari MH. Methanol steam reforming in a planar wash coated microreactor integrated with a micro-combustor. Int J Hydrogen Energy 2011;36:12822–32. https://doi.org/10.1016/j.ijhydene.2011.05.010.
[12] Tadbir MA, Akbari MH. Integrated methanol reforming and oxidation in wash-coated microreactors: a three-dimensional simulation. Int J Hydrogen Energy 2012;37:2287–97. https://doi.org/10.1016/j.ijhydene.2011.11.015.
[13] Gribovskiy AG, Makarshin LL, Andreev DV, Klenov OP, Parmon VN. A compact highly efficient multichannel reactor with a fixed catalyst bed to produce hydrogen via methanol steam reforming. Chem Eng J 2013;273:497–501. https://doi.org/10.1016/j.cej.2013.07.068.
[14] Gribovskiy AG, Makarshin LL, Andreev DV, Klenov OP, Parmon VN. Thermally autonomous microchannel reactor to produce hydrogen in steam reforming of methanol. Chem Eng J 2015;273:130–7. https://doi.org/10.1016/j.cej.2015.03.036.
[15] Ribeirinha P, Boaventura M, Lopes JCB, Sousa JM, Mendes A. Study of different designs of methanol steam reformers: experiment and modeling. Int J Hydrogen Energy 2014;39:19970–81. https://doi.org/10.1016/j.ijhydene.2014.10.029.
[16] Huang YX, Jang JY, Cheng CH. Fractal channel design in a micro methanol steam reformer. Int J Hydrogen Energy 2014;39:1998–2007. https://doi.org/10.1016/j.ijhydene.2013.11.088.
[17] Nehe P, Reddy VM, Kumar S. Investigations on a new internally-heated tubular packed-bed methanol-steam reformer. Int J Hydrogen Energy 2015;40:5715–25. https://doi.org/10.1016/j.ijhydene.2015.02.114.
[18] Peppley BA. A comprehensive kinetic model of methanol-steam reforming on $Cu/Zn/Al_2O_3$ Catalyst. Ph.D. Thesis. Kingston, Ontario, Canada: Royal Military College of Canada; 1997.
[19] Peppley BA, Amphlett JC, Kearns LM, Mann RF. Methanol-steam reforming on $Cu/ZnO/Al_2O_3$. Part 1: the reaction network. Appl Catal Gen 1999;179:21–9. https://doi.org/10.1016/S0926-860X(98)00298-1.
[20] Peppley BA, Amphlett JC, Kearns LM, Mann RF. Methanol-steam reforming on $Cu/ZnO/Al_2O_3$.Part 2: a comprehensive

kinetic model. Appl Catal Gen 1999;179:31–49. https://doi.org/10.1016/S0926-860X(98)00299-3.
[21] Das S. Study on coupling model of methanol steam reforming and simultaneous hydrogen combustion in micro-channel reactor. IOSR J Appl Chem 2015;8(1):20–5. https://doi.org/10.9790/5736-08122025.
[22] Chein R, Chen YC, Chung JN. Numerical study of methanol–steam reforming and methanol–air catalytic combustion in annulus reactors for hydrogen production. Appl Energy 2013;102:1022–34. https://doi.org/10.1016/j.apenergy.2012.06.010.
[23] Vadlamudi VK, Palanki S. Modeling and analysis of miniaturized methanol reformer for fuel cell powered mobile applications. Int J Hydrogen Energy 2011;36:3364–70. https://doi.org/10.1016/j.ijhydene.2010.12.062.
[24] Ghasemzadeh K, Liguori S, Morrone P, Iulianelli A, Piemonte V, Babaluo AA, Basile A. H_2 production by low pressure methanol steam reforming in a dense PdeAg membrane reactor in co-current flow configuration: experimental and modeling analysis. Int J Hydrogen Energy 2013;38:16685–97. https://doi.org/10.1016/j.ijhydene.2013.06.001.
[25] Lotric A, Sekavcnik M, Hocevar S. Effectiveness of heat-integrated methanol steam reformer and polymer electrolyte membrane fuel cell stack systems for portable applications. J Power Sources 2014;270:166–82. https://doi.org/10.1016/j.jpowsour.2014.07.072.
[26] Zhuang X, Xu X, Li L, Deng D. Numerical investigation of a multichannel reactor for syngas production by methanol steam reforming at various operating conditions. Int J Hydrogen Energy 2020;45:14790–805. https://doi.org/10.1016/j.ijhydene.2020.03.207.
[27] Heidarzadeh M, Taghizadeh M. Methanol steam reforming in a spiral-shaped microchannel reactor over $Cu/ZnO/Al_2O_3$ catalyst: a Computational Fluid Dynamics simulation study. Int J Chem React Eng 2017:15. https://doi.org/10.1515/ijcre-2016-0205.
[28] Lotric A, Sekavcnik M, Pohar A, Likozar B, Hocevar S. Conceptual design of an integrated thermally self-sustained methanol steam reformere-high-temperature PEM fuel cell stack manportable power generator. Int J Hydrogen Energy 2017;42:16700–13. https://doi.org/10.1016/j.ijhydene.2017.05.057.
[29] Mendes D, Chibante V, Zheng JM, Tosti S, Borgognoni F, Mendes A, Madeira LM. Enhancing the production of hydrogen via water-gas shift reaction using Pd-based membrane reactors. Int J Hydrogen Energy 2010;35:12596–608. https://doi.org/10.1016/j.ijhydene.2010.07.159.
[30] Chen WH, Syu YJ. Thermal behavior and hydrogen production of methanol steam reforming and autothermal reforming with spiral preheating. Int J Hydrogen Energy 2011;36:3397–408. https://doi.org/10.1016/j.ijhydene.2010.12.055.
[31] Augustine AS, Ma YH, Kazantzis NK. High pressure palladium membrane reactor for the high temperature water-gas shift reaction. Int J Hydrogen Energy 2011;36:3350–60. https://doi.org/10.1016/j.ijhydene.2011.01.172.
[32] Roses L, Manzolini G, Campanari S. CFD simulation of Pd-based membrane reformer when thermally coupled within a fuel cell micro-CHP system. Int J Hydrogen Energy 2010;35:12668–79. https://doi.org/10.1016/j.ijhydene.2010.07.080.
[33] Piemonte V, Falco MD, Favetta B, Basile A. Counter-current membrane reactor for WGS process: membrane design. Int J Hydrogen Energy 2010;35:12609–17. https://doi.org/10.1016/j.ijhydene.2010.07.158.
[34] Tosti S. Overview of Pd-based membranes for producing pure hydrogen and state of art at ENEA laboratories. Int J Hydrogen Energy 2010;35:12650–9.
[35] https://www.thermalfluidscentral.org/encyclopedia/index.php/.
[36] https://www.engineeringtoolbox.com/carbon-monoxide-d_975.html.
[37] https://webbook.nist.gov/cgi/cbook.cgi?ID=C67561&Mask=1#Thermo-Gas.
[38] https://www.engineersedge.com/heat_transfer/thermal-conductivity-gases.htm.
[39] Alfa Aesar: Product Bulletin: copper based methanol reforming catalyst HiFUELTM R120, Stock # 45468.
[40] Advent HT MEA Brochure. https://www.advent-energy.com/products-high-temperature-meas/.